This is the accepted version of the paper published online by Applied Physics Letters on 21 June 2022. The doi for this article is: https://doi.org/10.1063/5.0097172

Local anisotropy control of Pt/Co/Ir thin film with perpendicular magnetic anisotropy by surface acoustic waves[a)]

Jintao Shuai,[1] Mannan Ali,[1] Luis Lopez-Diaz,[2] John E Cunningham,[3] and Thomas A Moore[1]
[1)]*School of Physics and Astronomy, University of Leeds, Woodhouse Lane, Leeds, LS2 9JT, UK*
[2)]*Department of Applied Physics, Universidad de Salamanca, Salamanca, Spain*
[3)]*School of Electronic and Electrical Engineering, University of Leeds, Woodhouse Lane, Leeds, LS2 9JT, UK*

(Dated: 17 June 2022)

The control of perpendicular magnetic anisotropy (PMA) in thin films by strain has considerable potential for energy-efficient information storage and data processing. Here, we report on the control of PMA in Pt/Co/Ir thin films by the strain produced by standing surface acoustic waves (SAWs). A significant (∼21%) coercivity reduction (from 4.80 ± 0.03 mT to 3.80 ± 0.02 mT) can be obtained by applying a standing SAW with a centre frequency of 93.35 MHz. Furthermore, the standing SAWs induce a greater-than eleven-fold increase in magnetisation reversal speed (from 168 ± 3 μm^2/s to up to 2100 ± 80 μm^2/s) at 3.2 mT for a total applied RF power of 22.5 dBm. During application of SAWs, wide-field Kerr microscopy reveals the formation of domains in stripes with a periodicity of half of the SAW wavelength. Micromagnetic simulations indicate that the anti-nodes of the standing SAW locally lower the anisotropy due to the magneto-elastic coupling effect, decreasing domain nucleation field while promoting magnetisation reversal. Our study suggests the possibility of remote and energy-efficient control of magnetization switching using SAWs.

Please cite this article as DOI: 10.1063/5.0097172

Materials with strong perpendicular magnetic anisotropy (PMA) are promising candidates for future generations of data storage and processing devices owing to their stable magnetisation states and narrow domain walls.[1–4] These features confer stability of the stored information while providing a high storage density.[5] However, unfortunately materials with strong PMA typically also require a large current to reverse the magnetisation or to move domain walls in order to write or transfer data, which can itself cause energy wastage and Joule heating, so limiting the packing density of useful devices.[6,7] There is much interest in reducing the energy required to manipulate domain walls, for instance, by electric field or by strain.[8–13]

Owing to the magneto-elastic coupling effect, one can introduce strain to modify the PMA in a magnetic thin film by applying voltage to an adjacent piezoelectric material. For example, Shepley *et al* modified Pt/Co/Pt thin films with PMA by applying static strain using dc voltage applied to a piezoelectric transducer. The static strain reduced the coercivity, and increased the domain wall creep velocity by up to 100%.[14] De Ranieri *et al* demonstrated a 5% anisotropy reduction in out-of-plane anisotropy resulting in a 500% domain wall mobility variation in a perpendicularly magnetized GaMnAsP/GaAs ferromagnetic semiconductor by using a piezoelectric stressor.[15] Gopman *et al* reduced the coercivity of Co/Ni multilayers more than 30% by expanding the $Pb(Zr_{0.52}Ti_{0.48})O_3$ by 0.1%.[11]

Surface acoustic waves (SAWs) are acoustic waves traveling along the surface of a material exhibiting elasticity, which can introduce time-varying (dynamic) strain waves in the magnetic thin films.[16–21] Dean *et al* simulated the remote introduction of an array of attractive domain wall pinning sites by forming a standing strain wave showing theoretically that multiple domain walls could be synchronously moved by shifting the frequency of the SAW.[22] Adhikari *et al* reported that a SAW can depin magnetic domain walls, increasing the probability of depinning between 4-9 times, and increasing the domain wall velocity in Co/Pt multilayers up to 8 times.[19,20] Thevenard *et al* experimentally demonstrated up to 60% coercivity reduction in an out-of-plane magnetized (Ga,Mn)(As,P) films at ∼40 K, showing the potential of SAW-assisted magnetisation switching.[17] SAW-induced coercivity reduction and domain wall motion show significant potential for energy-efficient information storage and data processing devices, since the magnetisation switching is driven by voltage instead of current. However, the SAW-induced (dynamic strain) magnetisation switching mechanism of thin films with PMA remains unclear, especially the role of the nodes and anti-nodes of the standing SAW in the magnetisation reversal process. Besides, the correlation between the properties of SAWs and magnetisation changes also is uncertain.

In the current study, we demonstrate local anisotropy control of a Ta/Pt/Co/Ir/Ta thin film with PMA by standing SAWs at a centre frequency of 93.35 MHz. In the presence of a SAW, the coercivity of the thin films significantly decreases, while the magnetisation reversal speed increases. These experimental results along with micromagnetic simulations reveal that the anti-nodes of the standing SAWs locally reduce the anisotropy of the Pt/Co/Ir thin film, which lowers the coercivity and favours magnetisation reversal.

Fig.1 a and b shows a schematic of the experimental arrangement comprising a 2-mm-wide stripe of Ta(5.0)/Pt(2.5)/Co(1.1)/Ir(1.5)/Ta(5.0) (for nominal thick-

[a)]Authors to whom correspondence should be addressed: John E Cunningham, J.E.Cunningham@leeds.ac.uk; Thomas A Moore, T.A.Moore@leeds.ac.uk

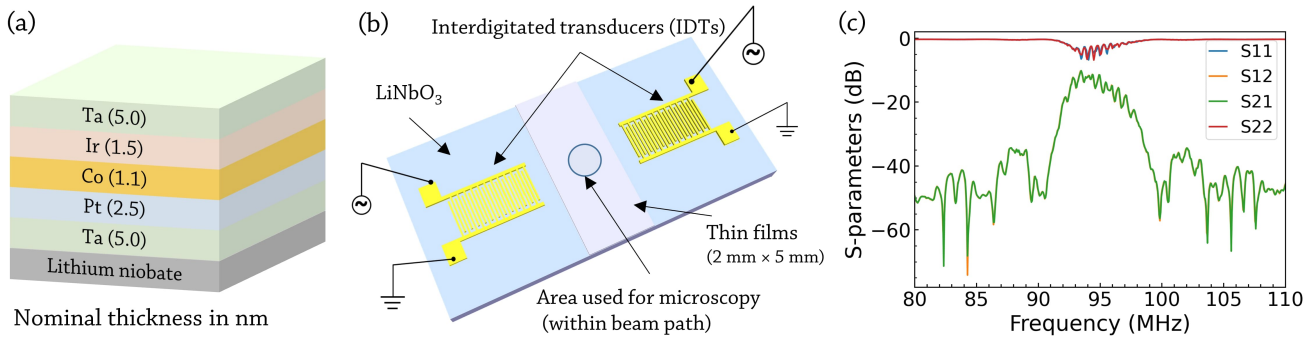

FIG. 1. (a) Thin film structure: Ta(5.0)/Pt(2.5)/Co(1.1)/Ir(1.5)/Ta(5.0) (nominal thickness in nm). (b) Schematic of experimental arrangement (not to scale). The 2-mm-wide thin film was dc sputtered onto the lithium niobate substrate. An interdigitated transducers (IDT) was patterned each side of the thin film to launch the SAWs. (c) Scattering parameters (S-parameters) of the interdigitated transducers. The delay line comprising both IDTs and the substrate shows a centre frequency of 93.35 MHz, and 3dB bandwidth of 9.34 MHz.

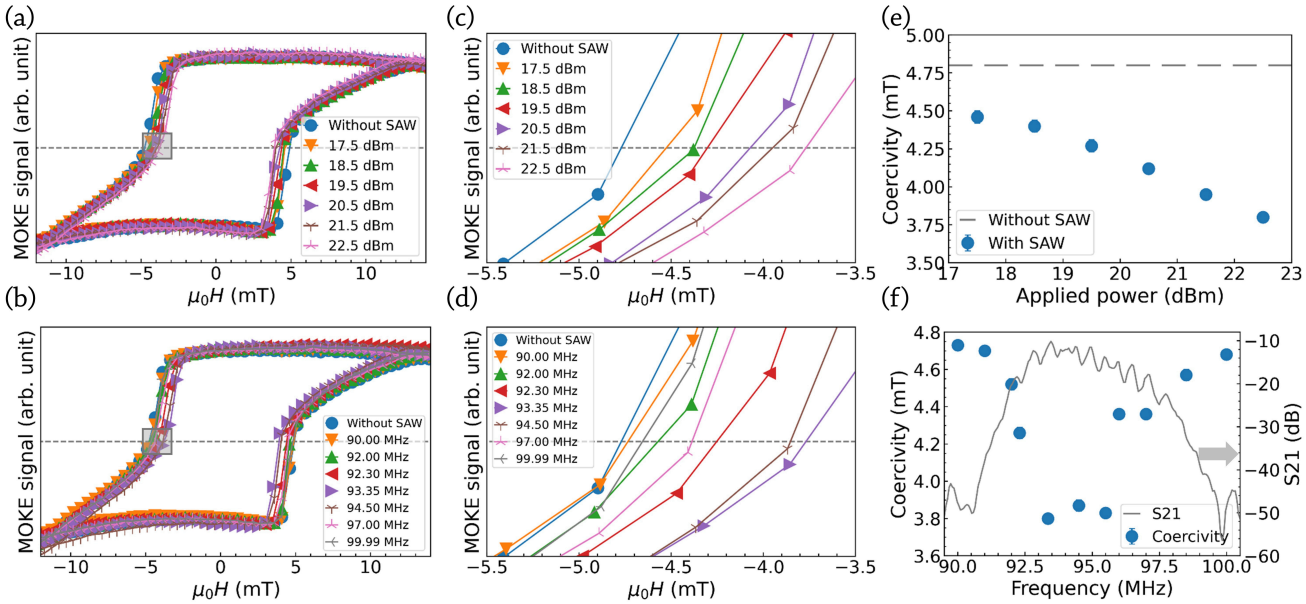

FIG. 2. Hysteresis loops of the thin films measured by Kerr microscopy across applied SAW power from 17.5 to 22.5 dBm (a) and SAW frequency from 90.00 to 99.99 MHz (b). (c) and (d) are the enlarged views of the framed areas in Fig. 2(a) and (b), respectively. Coercivity against applied power (e) and frequency (f). S21 is also displayed in (f). The frequency of SAW in (a), (c), and (e) is 93.35 MHz. The applied SAW power in (b), (d), and (f) is 22.5 dBm. Error bars in (e) and (f) are smaller than the data points. lines in (a) to (d) are guides to the eye.

nesses in nm, see Fig. 1a) thin film with PMA prepared by dc magnetron sputtering onto an 128° Y-cut lithium niobate ($LiNbO_3$) substrate. The base pressure during thin film preparation was below 3.0×10^{-6} Pa. As shown in Fig. 1b, one pair of Ti(10 nm)/Au(90 nm) interdigitated transducers (IDTs), each consisting of 20 pairs of electrodes, was patterned using optical lithography (exposure of the resist was achieved using a maskless laser aligner, with subsequent metal evaporation and lift-off forming the IDTs). The aperture of the IDTs and the SAW propagation distance were 450 μm and 3 mm, respectively. The finger width and spacing were both designed to be 10 μm. A vector network analyser (Agilent E5062A) was first used to obtain the S-parameters. Fig. 1c shows the reflection (S11 and S22) and transmission (S21 and S12) characteristics of the SAW transducers and substrate showing a centre frequency of 93.35 MHz, yielding a wavelength of 42.667 ± 0.004 μm (the accuracy of the frequency from VNA is 5ppm, and the propagating velocity of SAW on $LiNbO_3$ is 3982 m/s[23]). A description of the RF circuit used to apply signals to generate the SAWs is given in the supporting information. A wide-field Kerr microscope with a 50× objective lens and field applied out of the film plane was used to measure the hysteresis loops, image the domain patterns, and determine the magnetisation reversal speed of the thin films. To determine the magnetisation reversal speed, a pulsed field was applied to the thin film to switch the magnetisation, while

the magnetisation reversal speed was determined by the area of the reversed magnetisation divided by the pulse width. Details about the determination of magnetisation reversal speed can be found in supporting information. Five individual tests for all experiments were conducted and averaged.

Fig. 2a shows the hysteresis loops of the thin films for different applied SAW power from 17.5 to 22.5 dBm (at 93.35 MHz), and also without SAW. The sharp switching of the magnetisation indicates a strong perpendicular magnetic anisotropy of the Co layer. The presence of the curved corners is because a higher (than coercivity) field is required to squeeze out the homochiral domain walls to saturate the thin film.[24] Significant coercivity reduction was observed in the presence of the standing SAW: the coercivity decreases with increasing applied power from 4.46 ± 0.04 mT at 17.5 dBm to 3.80 ± 0.02 mT at 22.5 dBm (Fig. 2b and c). The coercivity is thus up to $\sim$21% reduced compared to that measured without SAW (4.80 ± 0.03 mT). The coercivity reduction can be explained by the strain-induced changes of the PMA.[14] SAWs act as time-varying strain waves, which can locally change the energy landscape of the thin films, periodically raising and lowering the anisotropy of the thin film. The magnetisation reverses when the anisotropy at low values. Due to the nature of the magnetisation reversal process, the magnetisation is not irreversible even when the anisotropy is at the highest value. The anisotropy changes increase with the increasing applied powers. It is worth noting that the introduction of the RF power used to generate the SAW could potentially increase the temperature, which could also lower the coercivity. We therefore investigated the effect of changing the frequency used to generate the SAWs for the same applied power level (Fig. 2d to f). The coercivity reduction gradually increases when the frequency approaches the centre frequency and reaches a minimum coercivity at the centre frequency following the same trend as the S21 curves (overlaid on the coercivity in Fig. 2f), thus indicating that the coercivity reduction is caused directly by the standing SAW instead of RF power induced heating. SAW-induced temperature changes are negligible, which has been reported in ref[17,25,26] using a similar setup and power level.

Fig. 3a to c shows the influence of the external field, applied SAW power and frequency of the SAW on the magnetisation reversal speed, respectively. As shown in Fig. 3a, with the external magnetic field increasing from 2.0 to 3.2 mT, the changes of the magnetisation reversal speed without SAW is very limited (from 71 ± 5 μm^2/s to 168 ± 3 μm^2/s), whereas, in the presence of the standing SAW, the magnetisation reversal speed increases from 249 ± 20 μm^2/s at 2.0 mT to 2100 ± 80 μm^2/s at 3.2 mT, which is a $\sim$740% increase. The magnetisation reversal speed is increased eleven-fold at 3.2 mT in the SAW's presence compared to that with magnetic field only. The implication is that the standing SAW can significantly lower the required switching field and accelerate the magnetisation reversal. At 93.35 MHz, the magnetisation reversal speed gradually increases with the increasing applied SAW power from 310 ± 30 μm^2/s at 17.5 dBm to 2100 ± 80 μm^2/s at 22.5 dBm with a 3.2 mT field (see Fig. 3b). Similar to the effect of frequency on the coercivity reduction, the magnetisation reversal speed increases when the frequency approaches the centre frequency, achieving its maximum value near the centre frequency (as shown in Fig. 3c). We note the S21 response is asymmetric and biased towards better transduction at lower frequencies, resulting in the biased magnetisation reversal speed. The change of the magnetisation reversal speed is caused by two main factors. Firstly, the presence of the standing SAW significantly reduces the domain nucleation field owing to the magneto-elastic coupling effect (see Fig. 2a). Meanwhile, the SAW induced anisotropy changes accelerate the domain wall velocity. The domain wall energy can be expressed as: $\gamma = \sqrt{AK_{eff}}$, where A is the exchange stiffness and K_{eff} is the effective anisotropy. SAW locally and periodically lower the anisotropy of the thin film, which benefits the domain wall motion.[14]

Fig. 4a and b shows domain patterns with both SAW on and off obtained using Kerr microscopy. A 50 mT out-of-plane magnetic field was first applied to the sample to saturate the magnetisation in the "up" direction. A 4.6 mT field was then applied in the opposite direction. A large number of small branch domains nucleated and propagated randomly in the thin film without the SAW (see Fig. 4a). With application of a standing SAW, the required domain nucleation field was much lower (around 3.6 mT for an applied power of 22.5 dBm at the centre frequency of 93.35 MHz). The domains tended to nucleate in certain parts of the thin film and line up forming a clear stripe pattern (as shown in Fig. 4b). The alignment of the domain patterns only occurs within the SAW beam path, with a random distribution of domains observed outside of the beam path (Fig. 4c). This result itself indicates very strongly that the standing SAWs are responsible for the domain patterns. Fig. 4e is cropped from Fig. 4b. By converting Fig. 4e into binary value (Fig. 4f) and counting the number of the black pixels, we plotted the distribution of the domains (see Fig. 4c). The experimental data was fitted by a sinusoidal function. The fit shows that the spacing between the lines is 20.88 ± 0.06 μm, corresponding well to the nominal half-wavelength ($\sim$21.33 μm) spacing expected of the standing SAW. This is because the magneto-elastic coupling effect will be the strongest at anti-nodes of the standing SAW, where the surface deflection is largest, and where the local lowering the anisotropy is expected to be the greatest. The effect is expected to be the weakest at the nodes of the standing SAW (as depicted in Fig. 4d).

To further understand the effect of the nodes and anti-nodes of the standing SAW on the magnetisation reversal process, we performed micromagnetic simulations using Mumax3 with a built-in strain tensor.[27] The configuration of the micromagnetic simulations can be found in supporting information. As shown in Fig. 5a, the red, white and blue indicate strains with maximum, zero, and minimum values, respectively. The system was firstly relaxed with magnetisation pointing "down" (see Fig. 5b). Standing SAWs ($\varepsilon_{max} = 0.06$) together with external magnetic field (300 mT) pointing "up" were then applied. As shown in Fig. 5c, at 1.5 ns, domains begin nucleating at the anti-nodes of the standing SAW. Then, the domains continue nucleating and propagating from anti-nodes to nodes until the domains merge with each other (Fig.

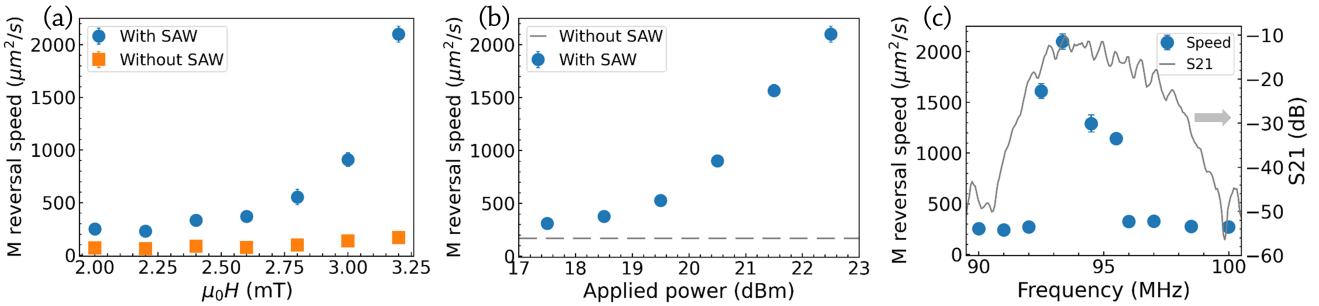

FIG. 3. Magnetisation reversal speed against external magnetic field (a), applied power (b) and frequency (c) of the standing SAW. The applied power and frequency of SAW in (a) are 22.5 dBm and 93.35 MHz, respectively. The external field and frequency of SAW in (b) are 3.2 mT and 93.35 MHz, respectively. The external field and applied power of SAW in (c) are 3.2 mT and 22.5 dBm, respectively.

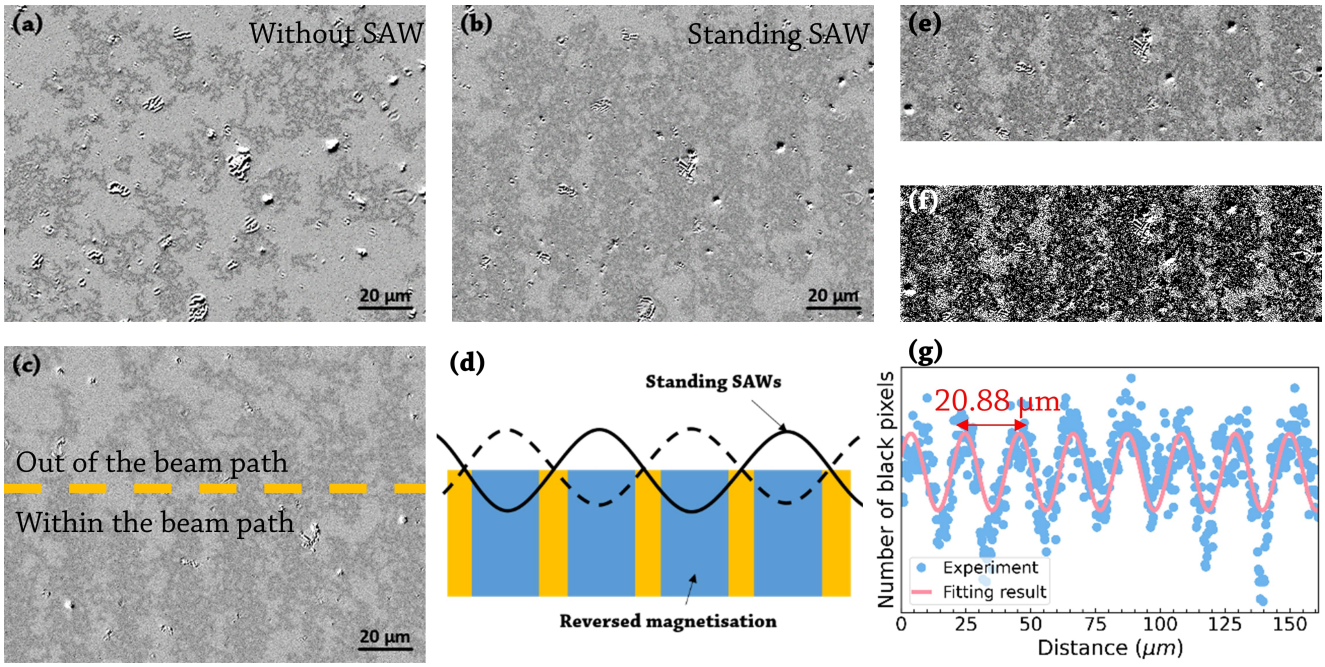

FIG. 4. (a) Domain patterns with only magnetic field (4.6 mT), (b) domain patterns with both magnetic field (3.6 mT) and 93.35 MHz standing SAW at 22.5 dBm, (c) domain patterns at the boundary of the beam path, (d) schematic of the standing SAW-assisted magnetisation reversal, (e) cropped image from Fig. 4b, (f) Fig. 4e in binary value, (g) the number of black pixels in Fig. 4f and its sinusoidal fitting. The fitting results show a wavelength of ∼20.88 μm, which is very close to the half-wavelength of the standing SAW (∼21 μm).

5d and e), followed by domain propagation out of the beam path (Fig. 5f). The simulation results agree qualitatively with our experiments and in particular our assumption that the anti-nodes of the standing SAW favour the nucleation of the domains and the propagation of the domain walls. The simulation and magnetisation reversal speed results also reveal that standing SAWs lower the coercivity of the thin films by lowering local domain nucleation field and accelerating domain wall propagation.

In conclusion, a strong coercivity reduction (up to $\sim 21\%$) was observed for the Ta/Pt/Co/Ir/Ta thin films with perpendicular magnetic anisotropy upon application of 93.35 MHz standing SAWs. Due to the SAW-induced magneto-elastic coupling effect, the magnetisation reversal speed was significantly enhanced (by a factor of 11). The experiments and Mumax simulations together indicate that, owing to the strain distribution difference, standing SAWs are able to lower the domain nucleation field locally at the anti-nodes of the standing SAW. Domains tended to nucleate and propagate from anti-nodes to nodes of the standing SAW, forming striped domain patterns with spacing the same as the half-wavelength of the standing SAW.

SUPPLEMENTARY MATERIAL

See supplementary material for RF circuit used to generate SAWs, determination of the magnetisation reversal speed and

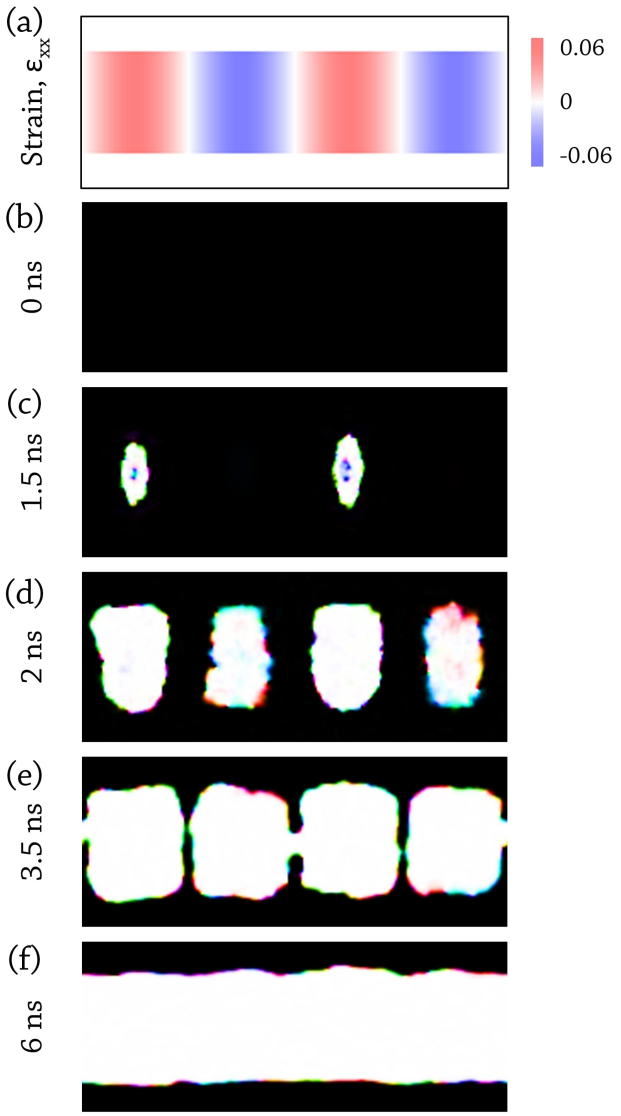

FIG. 5. (a) Spatial strain profile, (b) to (f) magnetisation at 0, 1.5, 2, 3.5 amd 6 ns after applying field (300 mT) and standing SAW. The black and white colors in (b) to (f) represent magnetisation pointing "down" and "up", respectively.

configuration of the micromagnetic simulations.

ACKNOWLEDGMENTS

The authors gratefully acknowledge funding from the European Union's Horizon 2020 research and innovation programme under the Marie Skłodowska-Curie grant agreement No. 860060 "Magnetism and the effect of Electric Field" (MagnEFi). The authors gratefully acknowledge Dr Li Chen for the interdigitated transducers fabrication.

[1] S.-W. Jung, W. Kim, T.-D. Lee, K.-J. Lee, and H.-W. Lee, "Current-induced domain wall motion in a nanowire with perpendicular magnetic anisotropy," Applied Physics Letters **92**, 202508 (2008).
[2] S. S. Parkin, M. Hayashi, and L. Thomas, "Magnetic domain-wall racetrack memory," Science **320**, 190–194 (2008).
[3] S. Emori, U. Bauer, S.-M. Ahn, E. Martinez, and G. S. Beach, "Current-driven dynamics of chiral ferromagnetic domain walls," Nature materials **12**, 611–616 (2013).
[4] K.-S. Ryu, L. Thomas, S.-H. Yang, and S. Parkin, "Chiral spin torque at magnetic domain walls," Nature nanotechnology **8**, 527–533 (2013).
[5] B. Dieny and M. Chshiev, "Perpendicular magnetic anisotropy at transition metal/oxide interfaces and applications," Reviews of Modern Physics **89**, 025008 (2017).
[6] I. M. Miron, T. Moore, H. Szambolics, L. D. Buda-Prejbeanu, S. Auffret, B. Rodmacq, S. Pizzini, J. Vogel, M. Bonfim, A. Schuhl, *et al.*, "Fast current-induced domain-wall motion controlled by the rashba effect," Nature materials **10**, 419–423 (2011).
[7] A. Yamaguchi, S. Nasu, H. Tanigawa, T. Ono, K. Miyake, K. Mibu, and T. Shinjo, "Effect of joule heating in current-driven domain wall motion," Applied Physics Letters **86**, 012511 (2005).
[8] F. Matsukura, Y. Tokura, and H. Ohno, "Control of magnetism by electric fields," Nature nanotechnology **10**, 209–220 (2015).
[9] G. Radaelli, D. Petti, E. Plekhanov, I. Fina, P. Torelli, B. Salles, M. Cantoni, C. Rinaldi, D. Gutiérrez, G. Panaccione, *et al.*, "Electric control of magnetism at the fe/batio3 interface," Nature communications **5**, 1–9 (2014).
[10] C. Song, B. Cui, F. Li, X. Zhou, and F. Pan, "Recent progress in voltage control of magnetism: Materials, mechanisms, and performance," Progress in Materials Science **87**, 33–82 (2017).
[11] D. B. Gopman, C. L. Dennis, P. Chen, Y. L. Iunin, P. Finkel, M. Staruch, and R. D. Shull, "Strain-assisted magnetization reversal in co/ni multilayers with perpendicular magnetic anisotropy," Scientific reports **6**, 1–8 (2016).
[12] Y. Shirahata, R. Shiina, D. L. González, K. J. Franke, E. Wada, M. Itoh, N. A. Pertsev, S. van Dijken, and T. Taniyama, "Electric-field switching of perpendicularly magnetized multilayers," NPG Asia Materials **7**, e198–e198 (2015).
[13] D. Bhattacharya, S. Bandyopadhyay, and J. Atulasimha, "Voltage induced strain control of magnetization: computing and other applications," Multifunctional Materials **2**, 032001 (2019).
[14] P. Shepley, A. Rushforth, M. Wang, G. Burnell, and T. Moore, "Modification of perpendicular magnetic anisotropy and domain wall velocity in pt/co/pt by voltage-induced strain," Scientific reports **5**, 1–5 (2015).
[15] E. De Ranieri, P. Roy, D. Fang, E. Vehsthedt, A. Irvine, D. Heiss, A. Casiraghi, R. Campion, B. Gallagher, T. Jungwirth, *et al.*, "Piezoelectric control of the mobility of a domain wall driven by adiabatic and non-adiabatic torques," Nature materials **12**, 808–814 (2013).
[16] W. Li, B. Buford, A. Jander, and P. Dhagat, "Acoustically assisted magnetic recording: a new paradigm in magnetic data storage," IEEE transactions on magnetics **50**, 37–40 (2014).
[17] L. Thevenard, I. S. Camara, J.-Y. Prieur, P. Rovillain, A. Lemaître, C. Gourdon, and J.-Y. Duquesne, "Strong reduction of the coercivity by a surface acoustic wave in an out-of-plane magnetized epilayer," Physical Review B **93**, 140405 (2016).
[18] W. Edrington, U. Singh, M. A. Dominguez, J. R. Alexander, R. Nepal, and S. Adenwalla, "Saw assisted domain wall motion in co/pt multilayers," Applied Physics Letters **112**, 052402 (2018).
[19] A. Adhikari and S. Adenwalla, "Surface acoustic waves increase magnetic domain wall velocity," AIP Advances **11**, 015234 (2021).
[20] A. Adhikari, E. Gilroy, T. Hayward, and S. Adenwalla, "Surface acoustic wave assisted depinning of magnetic domain walls," Journal of Physics: Condensed Matter **33**, 31LT01 (2021).
[21] Y. Cao, X. Bian, Z. Yan, L. Xi, N. Lei, L. Qiao, M. Si, J. Cao, D. Yang, and D. Xue, "Surface acoustic wave-assisted spin–orbit torque switching of the pt/co/ta heterostructure," Applied Physics Letters **119**, 012401 (2021).
[22] J. Dean, M. Bryan, J. Cooper, A. Virbule, J. Cunningham, and T. Hayward, "A sound idea: Manipulating domain walls in magnetic nanowires using surface acoustic waves," Applied Physics Letters **107**, 142405 (2015).
[23] J. Paskauskas, R. Rimeika, and D. Ciplys, "Velocity and attenuation of surface acoustic waves in proton-exchanged 128 degrees-rotated y-cut linbo3," Journal of Physics D: Applied Physics **28**, 1419 (1995).

[24]T. Nozaki, M. Konoto, T. Nozaki, H. Kubota, A. Fukushima, and S. Yuasa, "Control of the magnetic domain of pt/co/ru/mgo multilayer: Effect of co thickness and ru insertion," AIP Advances **10**, 035130 (2020).
[25]T. Yokouchi, S. Sugimoto, B. Rana, S. Seki, N. Ogawa, S. Kasai, and Y. Otani, "Creation of magnetic skyrmions by surface acoustic waves," Nature nanotechnology **15**, 361–366 (2020).
[26]L. Thevenard, I. S. Camara, S. Majrab, M. Bernard, P. Rovillain, A. Lemaître, C. Gourdon, and J.-Y. Duquesne, "Precessional magnetization switching by a surface acoustic wave," Phys. Rev. B **93**, 134430 (2016).
[27]A. Vansteenkiste, J. Leliaert, M. Dvornik, M. Helsen, F. Garcia-Sanchez, and B. Van Waeyenberge, "The design and verification of Mumax3," AIP Advances **4**, 107133 (2014).